Converting Between SMOS and SMAP Level-1 Brightness Temperature Observations Over Nonfrozen Land

Gabriëlle J. M. De Lannoy, Rolf H. Reichle, Jinzheng Peng, Yann Kerr, *Fellow, IEEE*, Rita Castro, Edward J. Kim, *Senior Member, IEEE*, and Qing Liu

***Abstract*—The Soil Moisture and Ocean Salinity (SMOS) and Soil Moisture Active Passive (SMAP) missions provide Level-1 brightness temperature (Tb) observations that are used for global soil moisture estimation. However, the nature of these Tb data differs: the SMOS Tb observations contain atmospheric and select reflected extraterrestrial ("Sky") radiation, whereas the SMAP Tb data are corrected for these contributions, using auxiliary near-surface information. Furthermore, the SMOS Tb observations are multiangular, whereas the SMAP Tb is measured at 40° incidence angle only. This letter discusses how SMOS Tb, SMAP Tb, and radiative transfer modeling components can be aligned in order to enable a seamless exchange of SMOS and SMAP Tb data in soil moisture retrieval and assimilation systems. The aggregated contribution of the atmospheric and reflected Sky radiation is, on average, about 1 K for horizontally polarized Tb and 0.5 K for vertically polarized Tb at 40° incidence angle, but local and short-term values regularly exceed 5 K.**

***Index Terms*—Atmosphere, brightness temperature (Tb), galaxy, soil moisture, Soil Moisture Active Passive (SMAP), Soil Moisture Ocean Salinity (SMOS).**

I. Introduction

SATELLITE-based L-band (1.4 GHz) microwave remote sensing is used for global soil moisture estimation by the Soil Moisture Ocean Salinity (SMOS) [1] mission and the Soil Moisture Active Passive (SMAP) [2] mission. To accurately interpret these L-band measurements in soil moisture retrieval algorithms [3] or data assimilation schemes [4], it is important to understand how the Earth surface, atmosphere, and extraterrestrial sources are contributing to the observed brightness temperature (Tb).

Both the SMOS and SMAP missions provide gridded Level-1 (L1) Tb data. However, the exact nature of the L1 Tb data is different, and they serve distinct Level-2 (L2) soil moisture retrieval algorithms. Specifically, the SMOS L1 Tb data are multiangular measurements that include Faraday rotation and contain atmospheric and select reflected extraterrestrial (i.e., cosmic and galactic, defined as "Sky" in Section IV) contributions. These contributions are consequently also included in the Tb forward modeling of the SMOS L2 soil moisture retrieval algorithm. In contrast, the SMAP L1B Tb data are measurements at 40° incidence angle with a lower measurement error, corrected for Faraday rotation, and corrected for atmospheric and Sky contributions using auxiliary near-surface information. The SMAP L2 retrieval algorithm therefore does not simulate the latter radiative contributions.

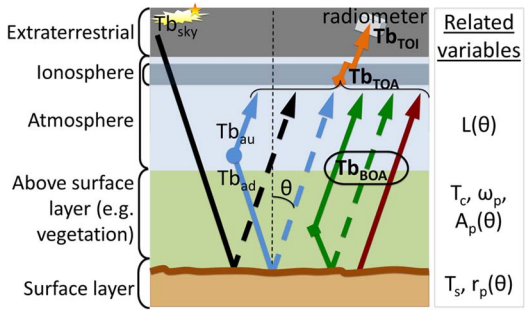

Fig. 1. Radiative sources and effects contributing to $\mathrm{Tb}_{\mathrm{BOA}}(\theta)$, $\mathrm{Tb}_{\mathrm{TOA}}(\theta)$, and the satellite-observed $\mathrm{Tb}_{\mathrm{TOI}}(\theta)$.

In this letter, we provide a discussion of how atmospheric and Sky contributions can be simulated in Tb forward modeling, removed from (multiangular) SMOS L1 Tb data, or added to the SMAP L1B Tb data, if so desired. It is also shown how the relatively noisy multiangular SMOS Tb data are converted into smoothed Tb estimates. This discussion arises from the need to enable a seamless exchange of SMOS and SMAP L1 Tb data in land data assimilation systems and retrieval algorithms.

II. Radiative Transfer Modeling

The antenna temperatures measured by the radiometers onboard spacecraft are Tb values at the top of the ionosphere $\mathrm{Tb}_{\mathrm{TOI},p}(\theta)$ [K], at polarization $p = (H, V)$ (horizontal, vertical), and incidence angle θ, convolved with the antenna pattern. We assume that the direct extraterrestrial radiation (Sun, Moon, and Sky; see Section IV) and reflected Sun and Moon radiation are removed from the satellite-based $\mathrm{Tb}_{\mathrm{TOI},p}(\theta)$. Fig. 1 illustrates that the $\mathrm{Tb}_{\mathrm{TOI},p}(\theta)$ is the Tb at the top of the atmosphere $(\mathrm{Tb}_{\mathrm{TOA},p}(\theta))$, altered through ionospheric Faraday rotation. The $\mathrm{Tb}_{\mathrm{TOA},p}(\theta)$ is composed of direct and reflected radiation

Manuscript received March 31, 2015; revised April 29, 2015; accepted May 19, 2015. Date of publication June 25, 2015; date of current version August 7, 2015. This work was supported by the NASA Soil Moisture Active Passive mission.

G. J. M. De Lannoy and J. Peng are with the NASA Goddard Space Flight Center, Greenbelt, MD 20771 USA and also with the Universities Space Research Association, Columbia, MD 21046 USA (e-mail: gabrielle.delannoy@nasa.gov).

R. H. Reichle and E. J. Kim are with the NASA Goddard Space Flight Center, Greenbelt, MD 20771 USA.

Y. Kerr is with the Centre d'Etudes Spatiales de la Biosphère, 31401 Toulouse, France.

R. Castro is with DEIMOS Engenharia, 1998-023 Lisboa, Portugal.

Q. Liu is with the NASA Goddard Space Flight Center, Greenbelt, MD 20771 USA and also with Science Systems and Applications, Lanham, MD 20706 USA.

Color versions of one or more of the figures in this paper are available online at http://ieeexplore.ieee.org.

Digital Object Identifier 10.1109/LGRS.2015.2437612

from the surface and vegetation (defined as Tb at the bottom-of-the-atmosphere, $\mathrm{Tb}_{\mathrm{BOA},p}(\theta)$), plus direct upwelling $\mathrm{Tb}_{\mathrm{au}}(\theta)$ and reflected downwelling $\mathrm{Tb}_{\mathrm{ad}}(\theta)$ atmospheric radiation, plus reflected Sky radiation $\mathrm{Tb}_{\mathrm{sky},p}(\theta)$, i.e.,

$$\begin{aligned}\mathrm{Tb}_{\mathrm{TOA},p}(\theta) = &\mathrm{Tb}_{\mathrm{BOA},p}(\theta)L(\theta)\cdots \\ &+ \mathrm{Tb}_{\mathrm{au}}(\theta) + \mathrm{Tb}_{\mathrm{ad}}(\theta)\left(1-\epsilon_{p,\mathrm{eff}}(\theta)\right)L(\theta)\cdots \\ &+ \mathrm{Tb}_{\mathrm{sky},p}(\theta)\left(1-\epsilon_{p,\mathrm{eff}}(\theta)\right)L(\theta)^2 \qquad (1)\end{aligned}$$

with

$$\begin{aligned}\mathrm{Tb}_{\mathrm{BOA},p}(\theta) = &T_s\left(1-r_p(\theta)\right)A_p(\theta)\cdots \\ &+T_c(1-\omega_p)\left(1-A_p(\theta)\right)\left(1+r_p(\theta)A_p(\theta)\right) \qquad (2) \\ \simeq &\epsilon_{p,\mathrm{eff}}(\theta)T_{s,\mathrm{eff}} \qquad (3)\end{aligned}$$

where T_s [K] is the surface soil temperature, T_c [K] is the canopy temperature, $r_p(\theta)$ [–] is the rough surface soil reflectivity, ω_p [–] is the scattering albedo, $A_p(\theta) = \exp(-\tau_p(0^\circ)/\cos(\theta))$ is the vegetation attenuation, $\tau_p(0^\circ)$ [–] is the nadir vegetation opacity, $L(\theta) = \exp(-\tau_{\mathrm{atm}}(0^\circ)/\cos(\theta))$ [–] is the atmospheric attenuation, and $\tau_{\mathrm{atm}}(0^\circ)$ [–] is the nadir atmospheric opacity. At L-band, it can be assumed that the downwelling and upwelling components of atmospheric radiation and opacity are identical and independent of the polarization [10]. Equation (2) is also known as the tau–omega model, which is commonly used to represent radiative transfer processes over land. Equation (3) assumes that the surface soil and canopy temperatures are equal (at thermal equilibrium, occurring approximately near 6:00 A.M. local time), and this effective temperature is denoted by $T_{s,\mathrm{eff}}$ [K]. The effective surface emissivity coefficient is $\epsilon_{p,\mathrm{eff}}(\theta)$ [–].

The SMOS L1 product provides footprint $\mathrm{Tb}^{\circ}_{\mathrm{TOI}}(\theta)$, where the superscript $^\circ$ refers to observations, along with the angles to perform Faraday rotation for the computation of $\mathrm{Tb}^{\circ}_{\mathrm{TOA}}(\theta)$. The SMAP L1B product provides footprint $\mathrm{Tb}^{\circ}_{\mathrm{BOA}}$ (40°) observations along with the values for the atmospheric and reflected Sky corrections, which enables the calculation of $\mathrm{Tb}^{\circ}_{\mathrm{TOA}}$ (40°). The following sections discuss the atmospheric and Sky corrections to derive $\mathrm{Tb}^{\circ}_{\mathrm{BOA}}(\theta)$ from $\mathrm{Tb}^{\circ}_{\mathrm{TOA}}(\theta)$ for multiangular SMOS observations. The same methods apply to update the corrections to the SMAP L1B data with customized auxiliary information or to adjust components of the radiative transfer modeling in retrieval or assimilation systems.

III. Tb Observations and Auxiliary GEOS-5 Background Fields

The SMOS L1 Tb data in this study are extracted from the MIR_SCLF1C product, with processor version 504 for the years 2010 and 2011 and version 505 from January 2012 onward [5]. Improved SMOS data versions will soon be available, but the methods described in this letter are independent of the data version. The various steps involved in the quality control and processing of the multiangular SMOS Tb data are described in [6]. The $\mathrm{Tb}^{\circ}_{\mathrm{TOI}}(\theta)$ data are transformed to $\mathrm{Tb}^{\circ}_{\mathrm{TOA}}(\theta)$, spatially mapped onto the 36-km Equal-Area Scalable Earth Grid version 2 (EASEv2) and binned per 1° incidence angle. Note that the SMOS L3 product also provides angularly binned Tb observations, and *simulated* Tb at the top of the atmosphere and the bottom of the atmosphere at 42.5° incidence angle only. These Tb simulations are produced with a forward radiative transfer model using retrieved soil moisture (and other retrieved variables). Here, we focus on transforming multiangular SMOS L1 Tb *observations* from the top of the atmosphere to the bottom of the atmosphere.

The auxiliary near-surface information used to correct atmospheric and Sky contributions consists of a subset of the following variables (depending on the method, see Section V): land surface elevation above mean sea level Z [km], land surface temperature T_s [K] (here using 5-cm soil temperature), 2-m air temperature T_a [K], 2-m surface water vapor density V_s [g/m^3], surface pressure P_s [mbar], and total precipitable water vapor content W [kg/m^2]. These dynamic background fields are based on atmospheric reanalysis data from the Goddard Earth Observing System version 5 (GEOS-5) Forward Processing for Instrument Teams [7]. Any other reanalysis product can be used, but our choice to use GEOS-5 reanalysis data will ensure Tb corrections that are consistent with our modeling system used for Tb data assimilation.

IV. Extraterrestrial Contributions

A. Concept

Extraterrestrial contributions to the satellite-observed Tb include the Sun, Moon, and Sky radiation emitted directly toward the antenna and indirectly by reflecting off the Earth's surface. The Sun contribution is removed from both the SMAP and SMOS L1 products. The Moon contribution is also corrected for in the SMAP L1B product, but this correction has been omitted for the SMOS L1 data over land, because of its negligible impact on soil moisture estimation.

The Sky radiation $\mathrm{Tb}_{\mathrm{sky},p}(\theta)$ at L-band includes the following: 1) constant cosmic background radiation of about 2.7 K; 2) variable hydrogen line emission, which is small except in the galactic plane where values around 3 K can occur; and 3) continuum radiation, which is considerably larger (more than 10 K) and strongest in the plane of the galaxy [8]. As the Earth completes its orbit around the Sun, it crosses the galactic plane twice, resulting in two peaks in the galactic noise per year. The magnitude of the peaks depends on the declination (or latitude, when projected on the Earth) of the spacecraft. Direct Sky radiation is removed from both the SMAP and SMOS L1 products. The reflected Sky radiation is also removed from the SMAP L1B product, but not from the SMOS L1 product. The reflected Sky radiation is instead accounted for in the SMOS L2 processing (retrieval algorithm) to keep model-dependent corrections apart from the SMOS L1 observations.

For the purpose of removing reflected Sky radiation from SMOS L1 data, we use precomputed Sky information [9] weighted with the SMOS antenna pattern after reflection on the surface (AUX_GAL_SM) at 0.25° resolution in both right ascension α and declination δ, as used in the forward Tb simulation of the SMOS L2 processor. For a given date, time, and position of the spacecraft, the celestial coordinates (α, δ) are calculated [8, Appendix C]) and $\mathrm{Tb}_{\mathrm{sky},H}(\theta)$ and $\mathrm{Tb}_{\mathrm{sky},V}(\theta)$ are looked up. The reflected Sky contribution is then calculated as the last term in (1), with the emissivity $\epsilon_{p,\mathrm{eff}}(\theta) = \mathrm{Tb}_{\mathrm{BOA},p}(\theta)/T_s$ (3) approximated by the ratio of the uncorrected L1 SMOS $\mathrm{Tb}^{\circ}_{\mathrm{TOA},p}(\theta)$ observations and the GEOS-5 surface temperature T_s (see Section III). The atmospheric attenuation $L(\theta)$ will be discussed in Section V.

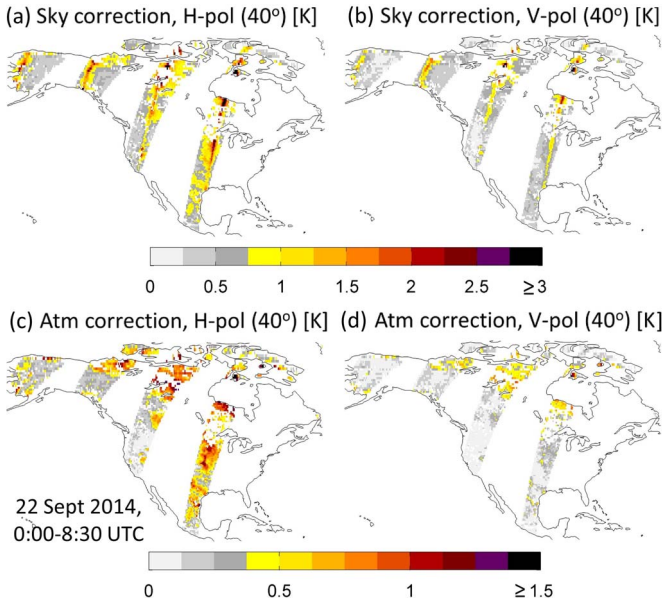

Fig. 2. Correction terms to convert $\mathrm{Tb}^{\circ}_{\mathrm{TOA}}(40^{\circ})$ to $\mathrm{Tb}^{\circ}_{\mathrm{BOA}}(40^{\circ})$ for descending SMOS Tb on September 22, 2014. (a) Reflected Sky radiation at H-polarization. (b) Same as (a) but at V-polarization. (c) Atmospheric corrections at H-polarization. (d) Same as (c) but at V-polarization.

The above procedure starts from $\mathrm{Tb}^{\circ}_{\mathrm{TOA},p}(\theta)$ data that are corrected for Faraday rotation, direct, and select reflected extraterrestrial radiation. Note that the SMAP L1B processor starts from antenna temperatures without any corrections other than for radiofrequency interference, and therefore, the estimate of the emissivity $\epsilon_{p,\mathrm{eff}}(\theta)$ is further tuned [11].

B. Example

Fig. 2(a) and (b) show examples of relatively high reflected Sky radiation ($\geq$3 K) in descending SMOS swaths on a day when the Earth is near the autumnal equinox. The typical along-track contributions vary in magnitude within the swath depending on the spacecraft position (sensor viewing geometry: pass direction, azimuth, and incidence angle) and the date and time of year. The correction is larger in the H-polarization, because $\epsilon_H(\theta) < \epsilon_V(\theta)$, while $\mathrm{Tb}_{\mathrm{sky},H}(\theta) \sim \mathrm{Tb}_{\mathrm{sky},V}(\theta)$.

V. Atmospheric Contributions

A. Concept

The atmosphere contributes through both upwelling and downwelling radiation, which is, in turn, reflected and attenuated by the soil, vegetation, and atmosphere (see Fig. 1). The atmospheric constituents contributing to microwave emission and absorption include oxygen, water vapor, clouds, and rain. At L-band wavelengths, the cloud contribution can be neglected. Light rain can also be neglected, and for high rain intensities ($> \sim$10 mm/h), Tb observations are typically flagged rather than corrected. The atmospheric contributions must thus be computed for oxygen and water vapor. Theoretically, the atmospheric opacity $\tau_{\mathrm{atm}}(\theta) = \tau_{\mathrm{atm}}(0^{\circ})/\cos(\theta)$, or its corresponding atmospheric attenuation $L(\theta) = \exp(-\tau_{\mathrm{atm}}(\theta))$, and the upwelling and downwelling radiative contributions $\mathrm{Tb}_{\mathrm{au}}(\theta) \simeq \mathrm{Tb}_{\mathrm{ad}}(\theta)$ can be estimated after integration over vertical profiles of temperature and pressure [10]. Table I lists three empirical

TABLE I
Three Empirical Models to Calculate $\tau_{\mathrm{atm}}(\theta)$ [Np] and $\mathrm{Tb}_{\mathrm{au}}(\theta)(\simeq \mathrm{Tb}_{\mathrm{ad}}(\theta))$ [K]. The Equations Require T_a in K, P_s in mbar, V_s in g/m^3, W in kg/m^2, and Z in km

SMAP atmospheric model for L1B data [10], [11]	
$\tau_{atm}(\theta)$	$= \ln[(1.00938 - 2.9626 \times 10^{-5}(T_a - 273.15) + 1.6521 \times 10^{-5}(P_s - 900) + 1.0712 \times 10^{-5} V_s)^{cos(40) sec(\theta)}]$
$\mathrm{Tb}_{au}(\theta)$	$= (2.3058 - 3.2735 \times 10^{-3}(T_a - 273.15) + 4.2330 \times 10^{-3}(P_s - 900) + 1.4472 \times 10^{-3} V_s) f(\theta)$
$f(\theta)$	$= 1.2855 \times 10^{-4}\theta^2 - 1.3361 \times 10^{-4}\theta + 0.7625$ (for $\theta < 20^{\circ}$)
$f(\theta)$	$= 8.2724 \times 10^{-6}\theta^3 - 5.7129 \times 10^{-4}\theta^2 + 2.0411 \times 10^{-2}\theta + 0.5655$ (for $20^{\circ} \leq \theta \leq 60^{\circ}$)
$f(\theta)$	$= 2.4189 \times 10^{-3}\theta^2 - 0.2458\theta + 7.5624$ (for $60^{\circ} < \theta \leq 70^{\circ}$)
SMOS atmospheric model for L2 soil moisture retrievals [3]	
$\tau_{atm}(\theta)$	$= \tau_{O_2}(\theta) + \tau_{H_2O}(\theta)$
$\tau_{O_2}(\theta)$	$= 10^{-6} \times (5.12341 \times 10^3 - 68.0605\ T_a + 24.2216\ P_s + 0.170616\ T_a^2 + 6.64682 \times 10^{-3}\ P_s^2 - 7.99404 \times 10^{-2}\ T_a\ P_s)/\cos(\theta)$
$\tau_{H_2O}(\theta)$	$= \max(0, (-113.724 + 0.155378\ P_s + 2.87254\ W) \times 10^{-6}/\cos(\theta))$
$\mathrm{Tb}_{au}(\theta)$	$= \mathrm{Tb}_{O_2}(\theta) + \mathrm{Tb}_{H_2O}(\theta)$
$\mathrm{Tb}_{O_2}(\theta)$	$= (T_a - \Delta T_{O_2})\tau_{O_2}(\theta)$
$\mathrm{Tb}_{H_2O}(\theta)$	$= (T_a - \Delta T_{H_2O})\tau_{H_2O}(\theta)$
ΔT_{O_2}	$= -3.16387 + 0.138628\ T_a + 3.29731 \times 10^{-3}\ P_s - 1.19886 \times 10^{-4}\ T_a^2 + 1.66366 \times 10^{-6}\ P_s^2 - 9.90743 \times 10^{-6}\ T_a\ P_s$
ΔT_{H_2O}	$= 8.07567 + 0.000516901\ P_s + 0.0344319\ W$
M3 model [12]	
$\tau_{atm}(\theta)$	$= \exp[-3.926 - 0.2211\ Z - 0.00369\ T_a]/cos(\theta)$
$\mathrm{Tb}_{au}(\theta)$	$= \exp[4.927 + 0.002195\ T_a](1 - \exp(-\tau_{atm}(\theta)))$

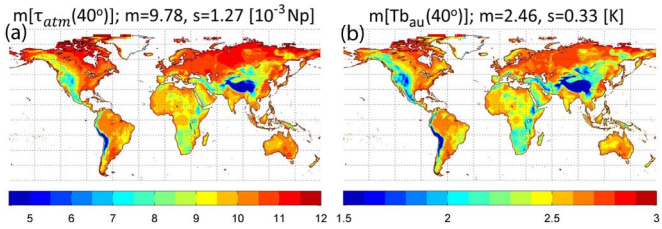

Fig. 3. Global four-year mean of SMAP estimates for (a) τ_{atm} (40°) and (b) $\mathrm{Tb}_{\mathrm{au}}$ (40°), July 1, 2010 to July 1, 2014.

models that have been used to estimate $\tau_{\mathrm{atm}}(\theta)$ and $\mathrm{Tb}_{\mathrm{au}}(\theta) \simeq \mathrm{Tb}_{\mathrm{ad}}(\theta)$: 1) equations used to correct SMAP L1B Tb observations [11]; 2) equations used in the Tb forward modeling of the SMOS L2 soil moisture retrieval algorithm [3]; and 3) equations proposed by [12], which are referred to as the M3 model here and have been used in global Tb forward modeling [6]. As input to these equations, we use the auxiliary fields of T_s, T_a, P_s, V_s, W, and Z provided by GEOS-5 simulations (see Section III).

Fig. 3 shows four-year averages of the SMAP estimates for τ_{atm} (40°) and $\mathrm{Tb}_{\mathrm{au}}$ (40°), with the lowest values occurring at higher elevations. The values for $\tau_{\mathrm{atm}}(\theta)$ decrease for smaller incidence angles (not shown), because of a reduced distance through the atmosphere. The temporal variability (not shown) is lowest in the tropics and increases with increasing seasonality toward the poles. Table II compares global four-year time series of estimates of τ_{atm} (40°) and $\mathrm{Tb}_{\mathrm{au}}$ (40°) by the three models. As in [10], both the τ_{atm} (40°) and $\mathrm{Tb}_{\mathrm{au}}$ (40°) estimates for model M3 show large biases, and thus also large root-mean-square-differences (rmsd), as compared with the SMAP and SMOS estimates, with τ_{atm} (40°) being underestimated and $\mathrm{Tb}_{\mathrm{au}}$ (40°) overestimated compared with the SMOS and SMAP estimates. In contrast, the biases between SMOS and SMAP estimates are very small. The global mean values ($\pm$global

TABLE II
GLOBAL MEAN AND STANDARD DEVIATION OF FOUR-YEAR STATISTICS FOR $\tau_{\rm atm}$ (40°) AND $\mathrm{Tb_{au}}$ (40°), JULY 1, 2010 TO JULY 1 2014. m[.] IS THE FOUR-YEAR MEAN, s[.] IS THE FOUR-YEAR STANDARD DEVIATION, BIAS IS THE FOUR-YEAR DIFFERENCE BETWEEN TWO MODEL ESTIMATES, RMSD IS THE ROOT-MEAN-SQUARE DIFFERENCE, AND CORR IS THE CORRELATION [–]

4-year statistic	global mean	global std-dev	global mean	global std-dev
	$\tau_{atm}(40^{\rm o})$ [Np]		$\mathrm{Tb}_{au}(40^{\rm o})$ [K]	
m[.] SMAP	9.78E-03	1.27E-03	2.46	0.33
m[.] SMOS	9.33E-03	1.47E-03	2.40	0.35
m[.] M3	6.10E-03	0.85E-03	3.39	0.27
s[.] SMAP	2.96E-04	1.43E-04	4.24E-02	2.06E-02
s[.] SMOS	5.62E-04	3.31E-04	6.49E-02	3.03E-02
s[.] M3	2.09E-04	1.18E-04	2.75E-02	1.48E-02
bias (SMAP-SMOS)	0.45E-03	0.39E-03	0.059	4.63E-02
bias (SMAP-M3)	3.68E-03	0.47E-03	-0.93	7.41E-02
rmsd (SMAP-SMOS)	0.66E-03	0.19E-03	0.071	4.00E-02
rmsd (SMAP-M3)	3.68E-03	0.46E-03	0.93	7.40E-02
	$\tau_{atm}(40^{\rm o})$ [-]		$\mathrm{Tb}_{au}(40^{\rm o})$ [K]	
corr (SMAP-SMOS)	0.98	1.43E-02	0.91	9.43E-02
corr (SMAP-M3)	0.94	7.25E-02	0.83	14.8E-02

standard deviation) for the rmsd are only $6.6 \pm 1.85 \times 10^{-4}$ Np between SMAP and SMOS estimates for $\tau_{\rm atm}$ (40°) and 0.07 ± 0.04 K for $\mathrm{Tb_{au}}$ (40°). Furthermore, the SMAP estimates for $\tau_{\rm atm}$ (40°) and $\mathrm{Tb_{au}}$ (40°) correlate very well with SMOS estimates and less well with M3 estimates. It can be assumed that the SMOS and SMAP models for atmospheric contributions are superior, since they were developed independently, by optimizing empirical expressions against multilayer atmospheric model simulations and radiosonde observations, respectively. The M3 model structure is much simpler, was based on a one-day global numerical weather forecast, and is therefore expected to be less accurate.

The atmospheric contributions can be removed from the Tb at the top of the atmosphere after removal of Sky radiation, i.e., $\mathrm{Tb}_{\mathrm{TOA-S},p}(\theta)$(= 2 first terms of (1), as discussed in Section IV), using (1) through (3), so that

$$\mathrm{Tb}_{\mathrm{BOA},p}(\theta) = T_s . \frac{\mathrm{Tb}_{\mathrm{TOA-S},p}(\theta) L(\theta)^{-1} - \left(1 + L(\theta)^{-1}\right) \mathrm{Tb}_{\mathrm{au}}(\theta)}{T_s - \mathrm{Tb}_{\mathrm{au}}(\theta)} \tag{4}$$

assuming again that $\mathrm{Tb}_{\mathrm{ad}}(\theta) = \mathrm{Tb}_{\mathrm{au}}(\theta)$. Occasionally, and particularly for V-polarization and higher incidence angles, $\mathrm{Tb}_{\mathrm{au}}(\theta)$ becomes large and $\mathrm{Tb}_{\mathrm{BOA},p}(\theta) > \mathrm{Tb}_{\mathrm{TOA-S},p}(\theta)$, which is purely an artifact of the empirical polynomials. In that case, we set $\mathrm{Tb}_{\mathrm{BOA},p}(\theta) = \mathrm{Tb}_{\mathrm{TOA-S},p}(\theta)$.

B. Example

An example of the atmospheric corrections ($= \mathrm{Tb}^{\circ}_{\mathrm{TOA-S},p}(\theta) - \mathrm{Tb}^{\circ}_{\mathrm{BOA},p}(\theta)$) to SMOS Tb is shown in Fig. 2(c) and (d). Unlike the Sky corrections [see Fig. 2(a) and (b)], atmospheric corrections are independent of the pass direction and azimuth angle of the spacecraft. Restructuring of (4) shows that the atmospheric correction is a negative function of the polarization-dependent $\mathrm{Tb}_{\mathrm{TOA-S},p}(\theta)$, and hence, the correction is larger for the smaller H-polarized Tb values than for the larger V-polarized Tb values. The corrections increase (decrease) with incidence angle for H-polarization (V-polarization).

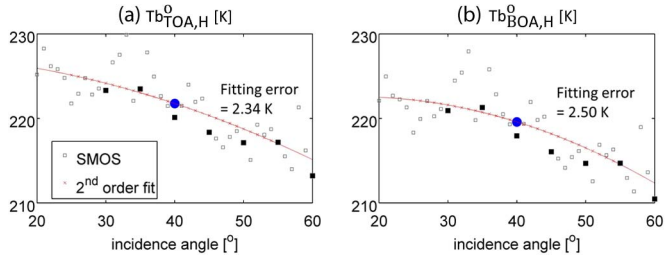

Fig. 4. Multiangular SMOS Tb (squares; filled squares highlight data at 30° through 60° with 5° intervals), along with the fitted counterparts (red crosses) and with indication of the fitted observation at 40° incidence angle (blue dot) at a location in Iowa (41.06° N, 95.41° W) for the descending swath around 01:00 UTC on September 22, 2014. (a) $\mathrm{Tb}^{\circ}_{\mathrm{TOA},H}(\theta)$ and (b) $\mathrm{Tb}^{\circ}_{\mathrm{BOA},H}(\theta)$ obtained after atmospheric and reflected Sky correction.

VI. ANGULAR FITTING

A. Concept

The SMAP Tbs have a radiometric error of ∼1.3 K but are only available at 40° incidence angle. By contrast, SMOS Tbs have a radiometric error of ∼4 K but are available for a range of incidence angles. This difference is rooted in the SMAP and SMOS instrument characteristics and complicates the use of SMOS observations in applications designed for SMAP. However, SMAP-like Tbs can readily be obtained from SMOS by interpolating the SMOS Tbs to the 40° incidence angle, as illustrated in this section. These "fitted" SMOS Tbs have lower errors and are convenient for use in applications designed for SMAP. At each grid cell and for each polarization separately, a quadratic curve is fitted through the multiangular 1° binned SMOS Tb between 20° and 60°, if observations are available for at least 15 angles, with at least 10 angles between 30° and 50°. The observations at each angle are weighted depending on the radiometric error, and the footprint is assumed identical for all angles. A quadratic curve adequately simulates the angular dependence of Tb and is highly efficient to process large data sets, because it involves a straightforward solution to a linear system. Note that Sky and atmospheric corrections require knowledge of the exact viewing geometry for each individual Tb observation, and consequently, the corrections need to be applied prior to the angular fitting.

B. Example

Fig. 4 shows an example of the angular fitting procedure for SMOS $\mathrm{Tb}^{\circ}_{\mathrm{TOA},H}(\theta)$ and $\mathrm{Tb}^{\circ}_{\mathrm{BOA},H}(\theta)$ at one location and one time step with relatively large atmospheric and reflected Sky corrections. The corrections reduce the values of the Tb observations and change the angular signature. The fitted observation for $\mathrm{Tb}^{\circ}_{\mathrm{BOA},H}$ (40°) is expected to be similar to a SMAP measurement, because it has a reduced (smoothed) error compared with the nonfitted original SMOS observations.

VII. COMPARISON OF LONG-TERM FITTED SMOS $\mathrm{Tb}^{\circ}_{\mathrm{TOA},p}$ (40°) AND $\mathrm{Tb}^{\circ}_{\mathrm{BOA},p}$ (40°)

The combined effect of the atmospheric and reflected Sky contributions is limited at the global and long-term scale. As discussed in Section VI, the larger Sky contributions are localized in space and time, whereas the atmospheric contributions

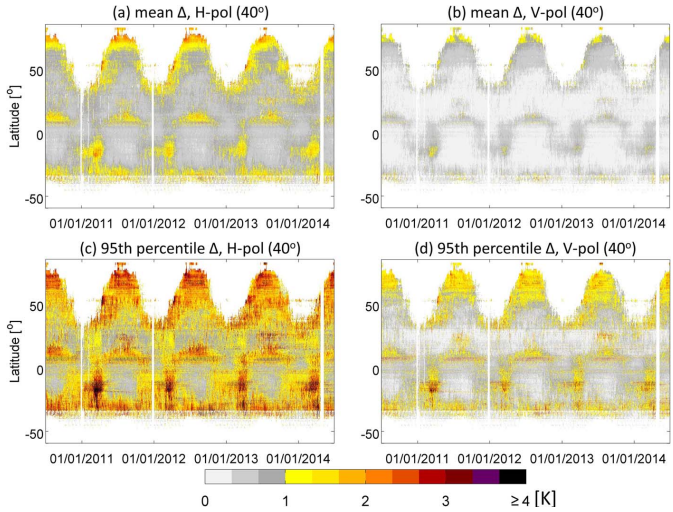

Fig. 5. Hovmöller plots of $\Delta = \mathrm{Tb}^{\circ}_{\mathrm{TOA},p} - \mathrm{Tb}^{\circ}_{\mathrm{BOA},p}$ at 40° incidence angle for fitted SMOS Tb and ascending swaths from July 1, 2010 through July 1, 2014. (a) Mean Δ for H-polarization. (b) Mean Δ for V-polarization. (c) Ninety-fifth percentile Δ for H-polarization. (d) Ninety-fifth percentile Δ for V-polarization.

are generally small (see Section V). Fig. 5(a) and (b) show a four-year smoothed time series of longitudinally averaged differences between the SMOS $\mathrm{Tb}^{\circ}_{\mathrm{TOA},H}$ and $\mathrm{Tb}^{\circ}_{\mathrm{BOA},H}$ fitted at 40° incidence angle for ascending swaths. Fig. 5(c) and (d) show the corresponding longitudinal 95th percentiles of the differences. The figures are similar for descending swaths. Overall, the mean differences are limited to less than 2 K in H-polarization and less than 1 K in V-polarization. The 95th percentile differences amount to values larger than 5 K at times with intense Sky radiation. The yearly pattern with the larger differences in the Southern Hemisphere for the months of March and April is related to Sky contributions.

VIII. Conclusion

L-band microwave measurements from the SMOS and SMAP missions enable frequently updated global estimates of soil moisture. To accurately interpret these Tb measurements, it is important to consider the exact radiative contributions included in the distributed L1 Tb data sets. For example, the SMOS L1 Tb data include atmospheric and reflected Sky radiation, whereas the SMAP L1B data are corrected for these contributions. When retrieving soil moisture from L1 Tb, the atmospheric and Sky radiation are explicitly modeled in the SMOS L2 product, whereas these contributions are not part of the SMAP L2 retrieval algorithm. In order to compare the SMOS or SMAP L1B Tb observations with radiative transfer modeling estimates in retrieval or assimilation systems, either the Tb data or the modeling estimates need to be adjusted to represent the same radiative information.

This letter presents steps to remove atmospheric and Sky contributions from SMOS L1 Tb observations at the top of the atmosphere in order to obtain Tb data at the bottom of the atmosphere, as provided by SMAP. In the process, we use auxiliary near-surface information from the GEOS-5 modeling system. The reflected Sky correction is calculated using precomputed celestial maps of Sky radiation, and an estimate of the emission coefficient given by the ratio of SMOS-observed Tb to simulated background information of surface temperature. The Sky contributions show distinct spatial patterns that change in time and space and depend on the position of the spacecraft. After removal of the reflected Sky radiation, the atmospheric contribution is removed using empirical formulas that use simulated background information of 2-m air temperature, 2-m water vapor density, surface pressure, and total precipitable water vapor content. A comparison of various atmospheric models reveals that the SMOS soil moisture retrieval (L2) processor and the SMAP L1B algorithm produce very similar estimates, whereas a third model by [12] introduces 1 K warm biases in the atmospheric radiation and overestimates the atmospheric opacity.

On average, the differences between Tb at the top of the atmosphere and the bottom of the atmosphere at 40° incidence angle are less than 2 K for H-polarization and less than 1 K for V-polarization. Local and short-term differences, however, regularly exceed 5 K. Moreover, the combined effect of Sky and atmospheric contributions causes differences in the spatial patterns and angular signatures between Tb measurements at the top of the atmosphere and the bottom of the atmosphere.

Acknowledgment

The authors would like to thank D. Le Vine and the reviewers for their helpful comments. Computational resources were provided by the NASA High-End Computing Program through the NASA Center for Climate Simulation at the Goddard Space Flight Center.

References

[1] Y. Kerr *et al.*, "The SMOS mission: New tool for monitoring key elements of the global water cycle," *Proc. IEEE*, vol. 98, no. 5, pp. 666–687, 2010.
[2] D. Entekhabi, S. Yueh, P. O'Neill, and K. Kellogg, "SMAP Handbook," Jet Propulsion Lab., Pasadena, CA, USA, pp. 400–1567, 2014.
[3] Y. Kerr, P. Walkteufel, P. Richaume, P. Ferrazzoli, and J.-P. Wigneron, "SMOS Level 2 Processor for Soil Moisture Algorithm Theoretical Basis Document (ATBD)" SM-ESL (CBSA), Toulouse, France, Tech Note SO-TN-ESL-SM-GS-0001 v1.3h, 2013.
[4] G. De Lannoy, P. de Rosnay, and R. Reichle, "Soil moisture data assimilation," in *Handbook of Hydrometeorological Ensemble Forecasting*, Q. Duan *et al.*, Eds. Berlin, Germany: Springer-Verlag, 2015.
[5] "SMOS data processors," Eur. Space Agency (ESA), Paris, France, 2015, https://earth.esa.int/web/guest/-/data-processors-7632
[6] G. De Lannoy, R. Reichle, and V. Pauwels, "Global calibration of the GEOS-5 L-band microwave radiative transfer model over non-frozen land using SMOS observations," *J. Hydrometeorol.*, vol. 14, pp. 765–785, 2013.
[7] R. Lucchesi, "File Specification for GEOS-5 FP-IT (Forward Processing for Instrument Teams)," Nat. Aeronaut. Space Admin. (NASA)/Goddard Space Flight Center (GSFC)/Global Modeling Assimilation Office (GMAO), Tech. Rep., 2013. [Online]. Available: https://gmao.gsfc.nasa.gov/pubs
[8] D. Le Vine and S. Abraham, "Galactic noise, and passive microwave remote sensing from space at L-band," *IEEE Trans. Antennas, Propag.*, vol. 42, no. 1, pp. 119–129, Jan. 2004.
[9] N. Floury, "Generation of a sky map to be used in Lvl1, and Lvl2 processors," European Space Agency (ESA), Paris, France, Tech. Note SO-TN-ESA-EEP-2009.412v3, 2013.
[10] J. Peng, E. Kim, and J. Piepmeier, "Global simplified atmospheric radiative transfer model at L-band," *IEEE Geosci., Remote Sens. Lett.*, vol. 10, no. 3, pp. 437–440, May 2013.
[11] J. Piepmeier *et al.*, "Algorithm theoretical basis document, SMAP L1B radiometer data product: L1B_TB," Nat. Aeronautics Space Admin., Jet Propulsion Lab., Washington, DC, USA, Tech. Rep., 2014.
[12] T. Pellarin *et al.*, "Two-year global simulation of L-band brightness temperatures over land," *IEEE Trans. Geosci. Remote Sens.*, vol. 42, no. 9, pp. 2135–2139, Sep. 2003.